Effect of annealing temperature on the structural, morphological, optical and electrical properties of Co3O4 thin film by nebulizer spray pyrolysis technique

Article *in* Journal of Materials Science Materials in Electronics · December 2015

DOI: 10.1007/s10854-015-4234-2

CITATIONS
5

READS
219

6 authors, including:

S. Valanarasu
Arul Anandar College
104 PUBLICATIONS **581** CITATIONS

SEE PROFILE

Kathalingam Adaikalam
Dongguk University
126 PUBLICATIONS **717** CITATIONS

SEE PROFILE

Effect of annealing temperature on the structural, morphological, optical and electrical properties of Co_3O_4 thin film by nebulizer spray pyrolysis technique

R. Manogowri, R. Mary Mathelane, S. Valanarasu, I. Kulandaisamy, A. Benazir Fathima & A. Kathalingam

Journal of Materials Science: Materials in Electronics

ISSN 0957-4522

J Mater Sci: Mater Electron
DOI 10.1007/s10854-015-4234-2

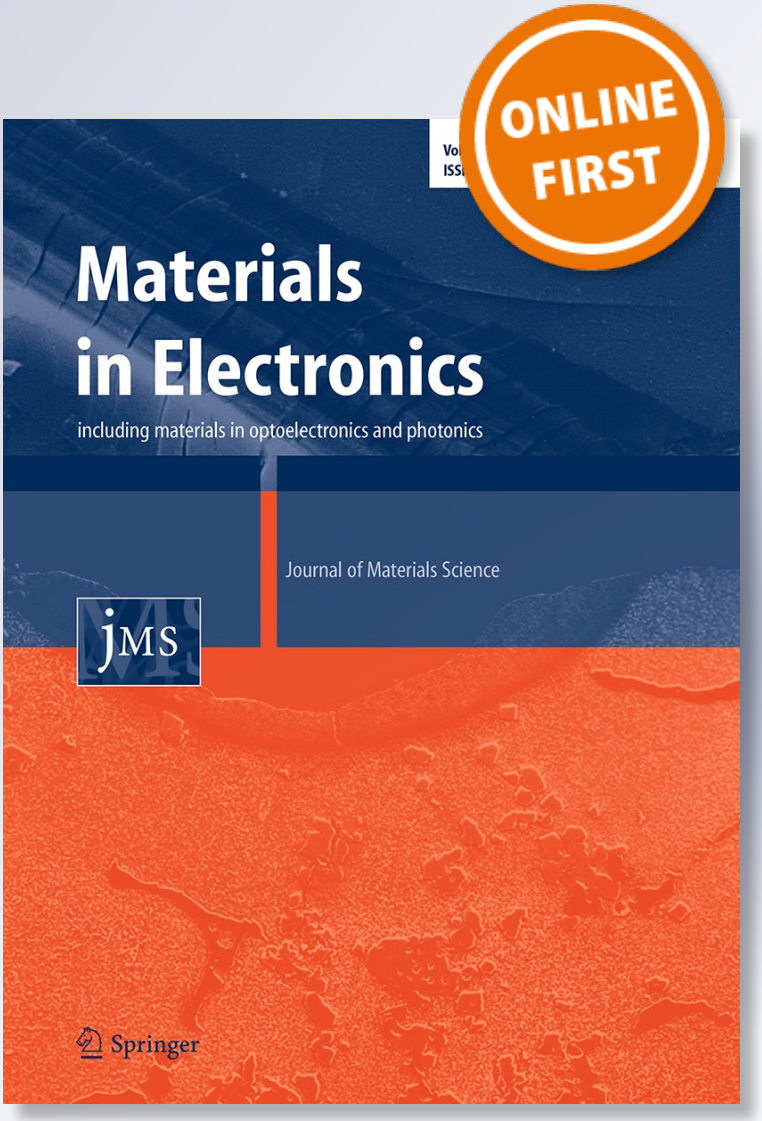

Springer

J Mater Sci: Mater Electron
DOI 10.1007/s10854-015-4234-2

Effect of annealing temperature on the structural, morphological, optical and electrical properties of Co_3O_4 thin film by nebulizer spray pyrolysis technique

R. Manogowri[1] · R. Mary Mathelane[1] · S. Valanarasu[2] · I. Kulandaisamy[2] · A. Benazir Fathima[1] · A. Kathalingam[3]

Received: 23 July 2015 / Accepted: 14 December 2015

Abstract In this investigation, spray pyrolysis using nebulizer technique is employed to fabricate cobalt oxide (Co_3O_4) thin films onto glass substrate at 250 °C. The deposited homogeneous Co_3O_4 thin films were thermally treated under different annealing temperatures. The influences of annealing temperature on the properties of the coated thin films are examined by XRD, SEM, EDAX, UV–Vis–NIR spectrometer and four probe techniques. XRD analysis confirmed the growth of polycrystalline cubic Co_3O_4 thin films. SEM analysis showed that the size of the spherical grains is increased with the increase of annealing temperature. The EDAX spectra have indicated that the grown film is in the composition of Co and O. The optical spectra has shown a decrease in transmittance for the increase of annealing temperature, and consequently the band-gap energy values are reduced as 2.26, 2.05 and 1.73 eV for as-deposited, annealed at 300 and 400 °C respectively. The optical constants like refractive index, extinction coefficient have also been determined from the optical measurements. Current versus voltage studies showed the ohmic nature of the films.

✉ R. Manogowri
rdharuni@gmail.com

[1] Jayaraj Annapackiam College for Women, Periyakulam 625601, India

[2] PG and Research Department of Physics, Arul Anandar College, Karumathur 625514, India

[3] Millimeter-Wave Innovation Technology Research Center (MINT), Dongguk University, Seoul 100-715, Republic of Korea

1 Introduction

Cobalt oxide (Co_3O_4) is a significant and versatile transition metal semiconductor oxide material. It has three recognized species [1]: cobaltous oxide (CoO), cobaltic oxide (Co_2O_3) and cobaltosic oxide (Co_3O_4). Relative to other two known phases, Co_3O_4 has more attention due to its potential application as an anodic electrochromic material [2], gas sensor [3], magnetic and supercapacitance material [4]. Co_3O_4 has been proposed as promoted catalyst in the decomposition of N_2O [5] and also as field emission material [6]. There are a range of traditional ways of manufacturing Co_3O_4 thin films such as chemical spray pyrolysis [7], metal organic chemical vapor deposition [8], pulsed spray evaporation [9], chemical bath deposition [10], sol–gel method [11], and spray pyrolysis [12]. Among these methods, the spray pyrolysis technique is facile and less expensive. Spray pyrolysis using nebulizer technique is a very easy, low cost, safe and non-vacuum system. This technique has advantage where atomization is done based on hydraulic pressure without any carrier gas, thereby performing occasional spraying leads to fine atomization of the given material. Nebulizer spray pyrolysis technique has a good control over the material use, so that with the minimum use of materials good quality films can be produced [13]. For uniform deposition, researchers usually modify the spray nozzle. Raj et al. [14] has employed a rotating sprayer with a swing motion, which resulted in similar films with clonable properties. Sethupathi et al. [15] applied a method that preheats the spray smog which is isolated from the substrate heater. Marikannu et al. [16] has produced thin films with preferential properties, via jet nebulizer spray pyrolysis technique. For the deposition process, we made mechanical arrangements to displace the nozzle in the x–y directions above the substrate, which is

Published online: 26 December 2015

useful to grow the films with uniform thickness over a large surface area. While screening the literature, it is found no study has tried to prepare Co_3O_4 material via nebulizer spray pyrolysis technique. Therefore, in this work, Co_3O_4 thin films were fabricated via nebulizer spray pyrolysis technique and the study on the impact of different annealing temperatures on the structural, morphological, optical, and electrical properties of Co_3O_4 films was carried out.

2 Experimental

Prior to the film deposition the glass substrates were first cleaned with distilled water and detergent, followed by chromic acid and finally soaked with acetone then the substrates were warmed by a hot air dryer, which makes assurance for uniform coating at all exposed surfaces. Experimental setup of spray pyrolysis using nebulizer is shown in Fig. 1. Nanosized Co_3O_4 thin films have been synthesized by a spray pyrolysis using nebulizer technique from 0.1 M aqueous solution of cobalt acetate tetra hydrate $Co(CH_3COO)_2{\cdot}4H_2O$ onto the glass substrates. During the film deposition, the substrate temperature was kept at 250 °C . The volume of the solution used for each deposition was 5 ml. Only small amount of solution was consumed and 10 min was necessary for spraying 5 ml i.e., 0.5 ml min^{-1}. The nozzle to substrate distance was ~5 cm and the optimized air flow rate was 1.5 kg cm^{-2}. After deposition of the material, the films were left to cool slowly to room temperature. The properties of the obtained Co_3O_4 thin films were studied with as-deposited, annealed at 300 and 400 °C . Thickness of the film was begun to increase due to enlargement in the grain size as a consequence of annealing temperatures, and is confirmed by the profilometry analysis and is shown in Table 1.

Table 1 Thickness values of Co_3O_4 thin films prepared by spray pyrolysis using nebulizer technique

Annealed	Thickness (μm)
As deposited	0.37
300 °C	0.39
400 °C	0.42

3 Results and discussions

3.1 X-ray diffraction analysis

Structural properties of the Co_3O_4 thin films were studied by using X-ray diffraction (XRD) technique. The XRD patterns of Co_3O_4 thin films with different annealing temperatures are shown in Fig. 2. It was found that all the samples are polycrystalline with Co_3O_4 cubic phase; no other phases could be detected. After film formation, no other structural changes have been observed, indicating that Co_3O_4 phase is stable and homogeneous. The good agreement between observed and standard d values is seen from ASTM data file no. (9-418). A thin film annealed at 400 °C displays major XRD peak corresponding to (311) and (222) planes also get enhanced. This justifies that Co_3O_4 phase and its formation is dependent of annealing temperature. The mean grain size, D was calculated using Debye Scherer's formula:

$$D = \frac{0.9\lambda}{\beta \operatorname{Cos} \theta} \tag{1}$$

where λ is wavelength of X-rays (1.5406×10^{-10} m) and β the full width in radian at half maximum of the peak and θ is Bragg's angle of XRD peak. The grain size is found to be varied from 2 to 5 nm as annealing temperature was increased. The nonexistence of the noisy background observed in Fig. 2 evidently signifies the existence of orderly formation of fine grains and it further strengthen the fact that these films are nanocrystalline in nature.

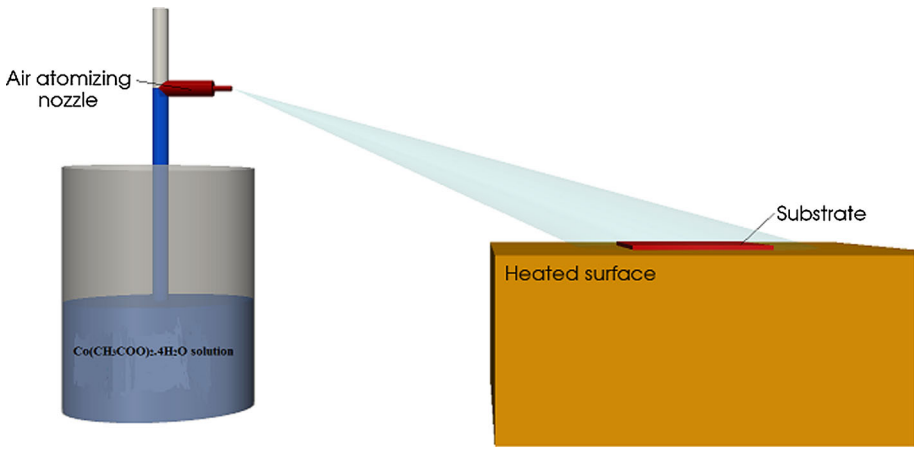

Fig. 1 Experimental setup of spray pyrolysis using nebulizer technique

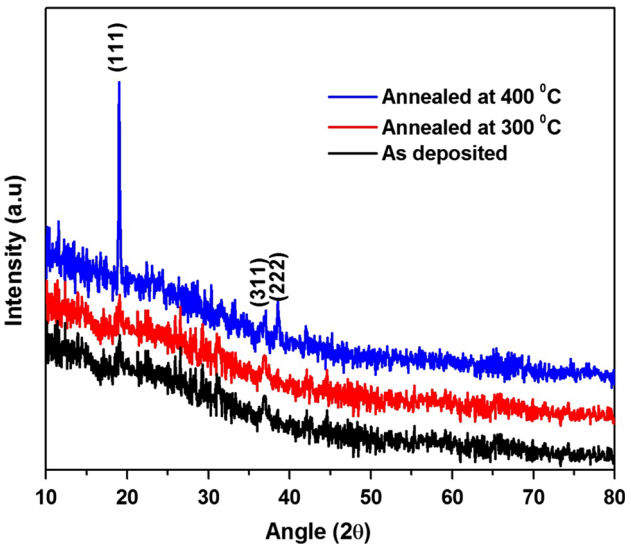

Fig. 2 The XRD patterns of Co_3O_4 thin films prepared by spray pyrolysis using nebulizer technique

3.2 Surface morphological studies

The scanning electron microscopy (SEM) images of the synthesized Co_3O_4 films are represented in Fig. 3. It indicated that all the films exhibited well dispersed spherical grains. The SEM images show that the grown films are uniform covering the whole substrate with nano-size grains. The annealed films found to show enhancement in grain size and inter-grain connectivity. The elemental analysis of the Co_3O_4 films was carried out using the EDAX. The typical EDAX spectra of the Co_3O_4 films are shown in Fig. 4. It is evident that presence of both Co and O with sufficient amount implies the formation of oxide in the synthesized samples. In the entire scanning range of binding energies, no observable peak belonging to impurity is perceived. The wt% of each (Co and O) decreases with the increase of annealing temperature indicating the grain enlargement, which is in agreement with the SEM pictures. Such surface morphology may offer expanded surface area, beneficial for super capacitor and gas sensing applications [17].

3.3 Optical studies

Optical transmittance of the Co_3O_4 films at different annealing temperatures is shown in the Fig. 5. The optical transmittance spectrum is recorded from 300 to 800 nm wavelength regions. When the films were undergone for annealing temperatures, the transmittance values found to decrease. The decrease is more significant when the films are exposed in annealing at 400 °C present an absorption peak at $\lambda = 740$ nm, which corresponds to a charge transfer ligand–metal $O^{2-} \rightarrow Co^{3+}$. The peak corresponds to $\lambda = 680$ nm by the virtue of Co^{2+}. These transitions confirm the existence of Co_3O_4. The transmittance of the Co_3O_4 films at different annealing temperatures is fairly about 31–41 % for the wavelengths in the UV–Vis regions, while that of transmittance of all the Co_3O_4 films however high about 60–82 % in the near infrared region. The range of optical transmittance in these films prescribes that the deposited films will be useful in reinforcing the performances of optoelectronic devices like photo detectors having sensitivity in the Visible to near infra-red wavelength region [18]. The absorbance of Co_3O_4 films at different annealing temperatures is about 38–50 % in the wavelength region of UV–Vis; these are evident in Fig. 6 which gives a plot of absorbance versus wavelength. The absorbance of all the films, nevertheless, reduced to low values about 22–8 % in the NIR region. The low absorbance in the UV–Vis region for as deposited film can be associated to crummy crystalline structure of the films. The

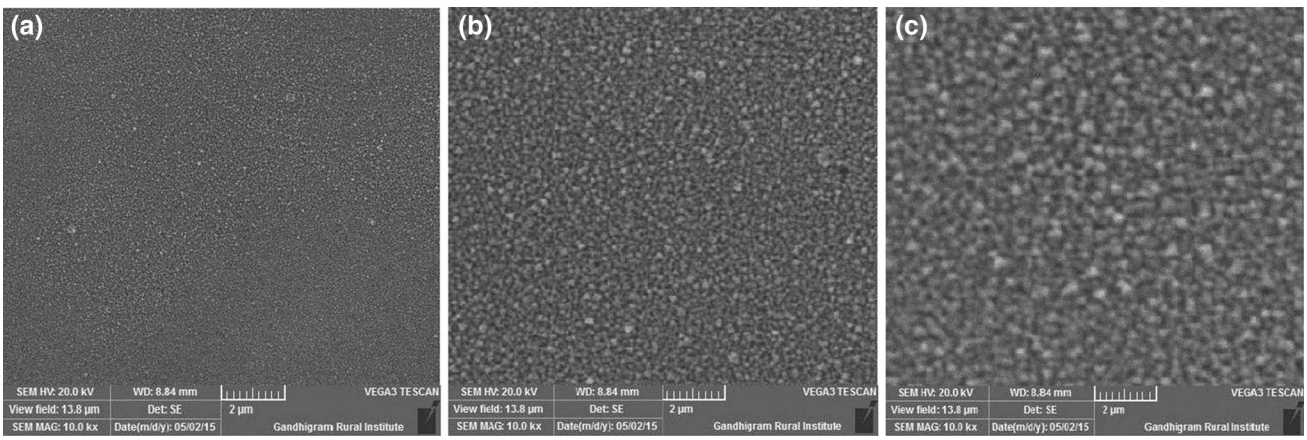

Fig. 3 SEM images of Co_3O_4 thin films **a** as deposited, **b** annealed at 300 °C, **c** annealed at 400 °C

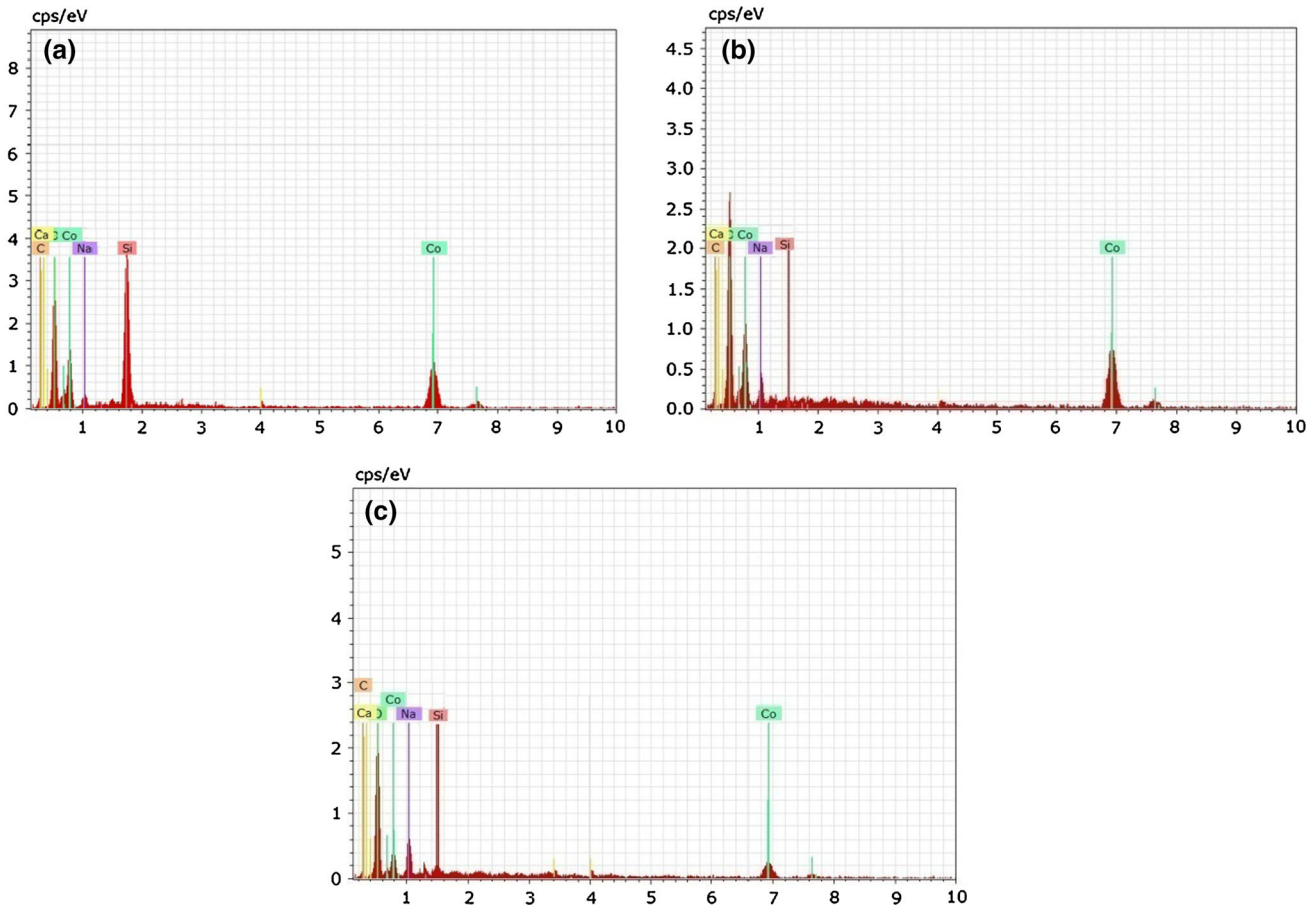

Fig. 4 EDAX spectra for Co_3O_4 thin films **a** as deposited, **b** annealed at 300 °C, **c** annealed at 400 °C

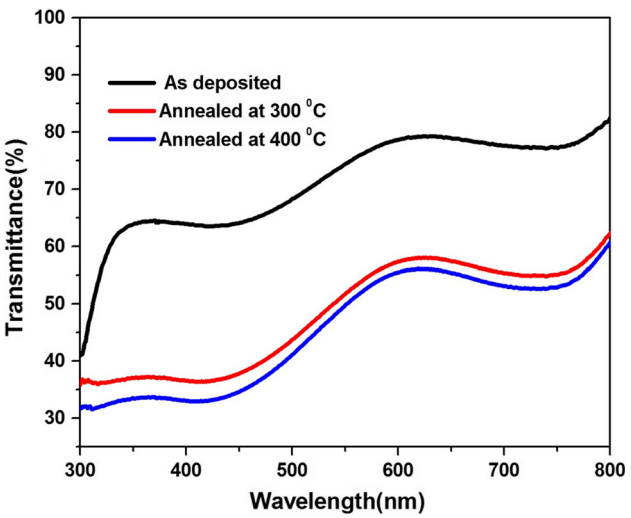

Fig. 5 Transmittance spectra of Co_3O_4 thin films annealed at different temperatures

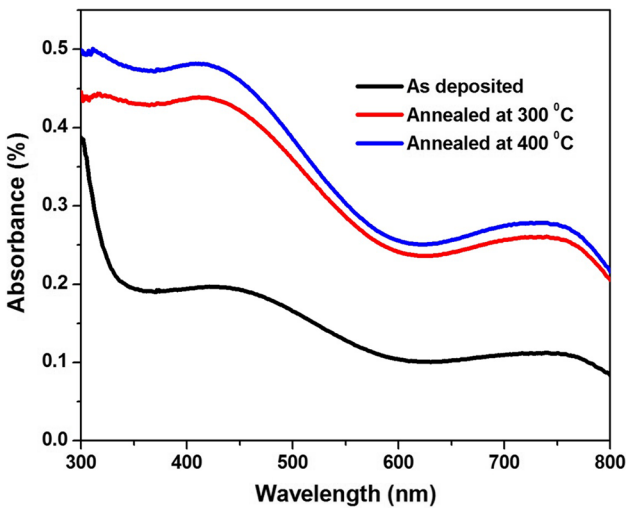

Fig. 6 Absorption spectra of Co_3O_4 thin films annealed at different temperatures

films are observed to show better crystallization, due because of absorption of the more of the incident radiation and annealing at higher temperatures. Figure 7 depicts the absorption coefficient as a function of photon energy. The absorption coefficient (α) value is able to determine from the formula,

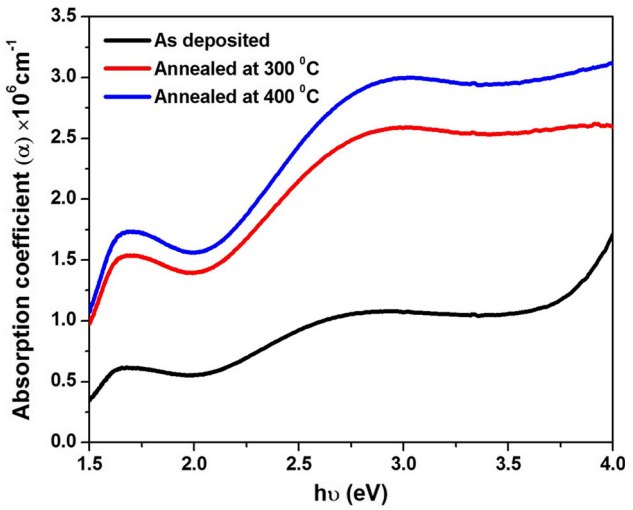

Fig. 7 Absorption coefficient of Co_3O_4 thin films annealed at different temperatures

$$\alpha = \frac{2.303\,A}{t} \tag{2}$$

where α is the absorbance and t is the thickness of the film. The absorption coefficient increase is found to with increasing annealing temperature. This can be demonstrated according to an increase in order of crystalline as the annealing temperatures increased. Figure 8 shows plots of $(\alpha h\upsilon)^2$ as a function of photon energy $(h\upsilon)$ for Co_3O_4 thin films as a function of annealing temperature. Since the plots are moreover linear, where, the direct nature of the optical transition in Co_3O_4 is ratified. Estimation of these curves to photon energy axis confesses the band gaps. The optical absorption data were interpreted using the following classical relation for near edge optical absorption in semiconductor.

$$\alpha = \frac{\alpha_0\,(h\upsilon - E_g)^n}{h\upsilon} \tag{3}$$

where α_0 is a constant, E_g is the semiconductor band gap and n is a number equal to ½ for direct gap and two for indirect gap compound.

The band gap of Co_3O_4 film was found to be decreased from 2.26 to 1.77 eV for films annealed at different temperatures. The resulting band gap values are almost good in agreement with the reported Co_3O_4 band structure of Drasovean et al. [19] and Balouria et al. [20]. The falloff in E_g with annealing temperature might be as a result of increase in crystalline size and reduction of defect sites. Figure 9 shows the variation of refractive index as a function of wavelength. The values decay exponentially with increasing wavelength. This indicates that the electromagnetic radiation passing through the material is slower in the UV and Vis regions near the UV–Vis boundary. However, the speed is higher in the Vis and near infra-red (NIR) regions. Refractive index values can be determined from the formula,

$$n = \sqrt{\frac{4R}{R-1} - (k^2)} - ((R+1)/(R-1)) \tag{4}$$

where R is the reflectance and k is the extinction coefficient. The refractive index of the films could be seen to range from 1.44 to 2.30. Thin films with refractive index approximately 1.9 have been reported to be employable as anti reflecting material [21]. The as-deposited film has refractive index nearer to the value of aforestated energy range, it can be handled for this purpose. It also shows that

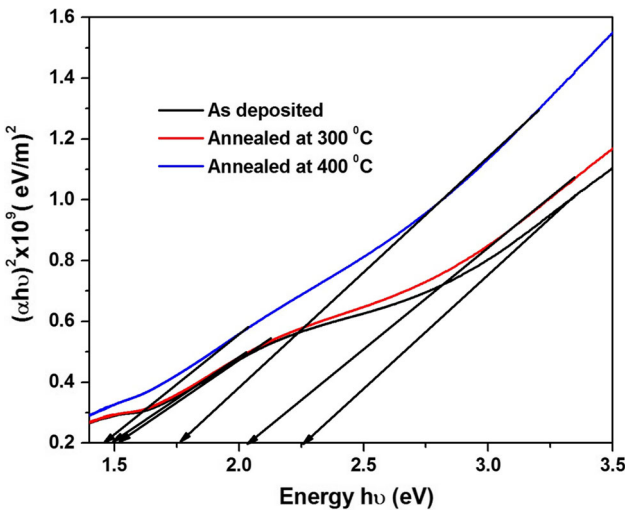

Fig. 8 Plot of $(\alpha h\upsilon)^2$ versus $(h\upsilon)$ of Co_3O_4 thin films annealed at different temperatures

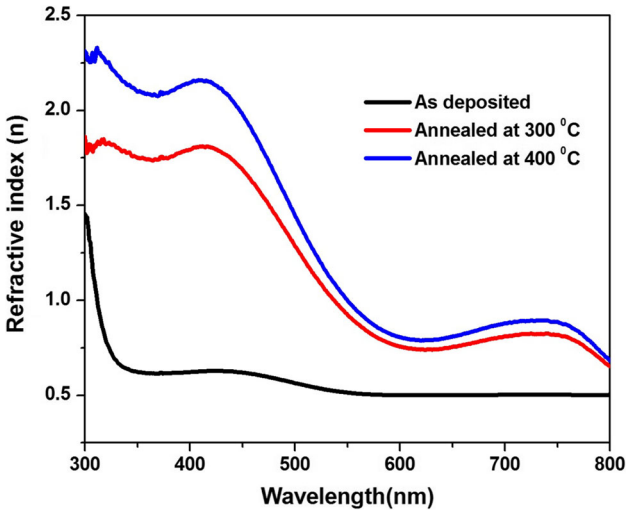

Fig. 9 Refractive index versus dispersion of Co_3O_4 thin films annealed at different temperatures

refractive index of the films upgraded with increase in annealing temperature that to non-gradually.

Figure 10 shows the plot of extinction coefficient as a function of wavelength. The extinction value can be obtained from the relation,

$$K = \frac{\alpha\lambda}{4\pi} \tag{5}$$

The increase in k value with increase in annealing temperature as a result of surface of the film, which intensified the scattering losses by that diminishing the transmitting ability. This conjecture is true with our observed optical transmittance spectra. In general, the index of refraction has dropped off monotonically with increasing wavelength. Further, it may be mentioned that the refractive index and extinction coefficient relay upon the atomic density and atomic masses of each intrinsic element. The refractive index is always immense for crystalline material. This is due to the lower atomic density of each element in the amorphous state because of the higher average interatomic distance. The skin depth (χ) can be obtained from the formula,

$$\chi = \frac{\lambda}{2\pi k} \cdot \tag{6}$$

Figure 11 represent the relationship between skin depths versus wavelength. From this depiction, it can be seen that the depth of light penetrated in the thin film is transmittance oriented. Figure 12 shows the plot between optical conductivity with the wavelength. Optical conductivity values were obtained from the formula (5).

$$\sigma = \frac{\alpha nc}{4\pi} \tag{7}$$

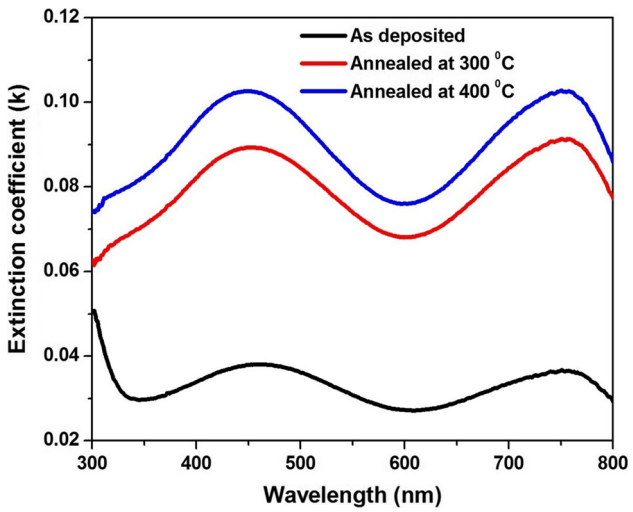

Fig. 10 Extinction coefficient of Co_3O_4 thin films annealed at different temperatures

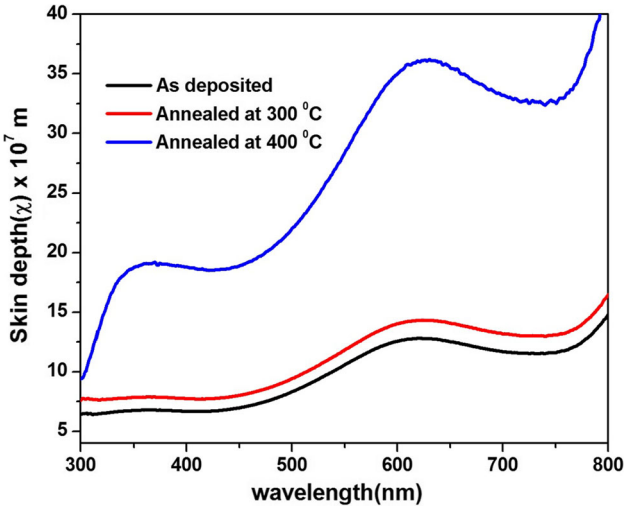

Fig. 11 Skin depth of Co_3O_4 thin films annealed at different temperatures

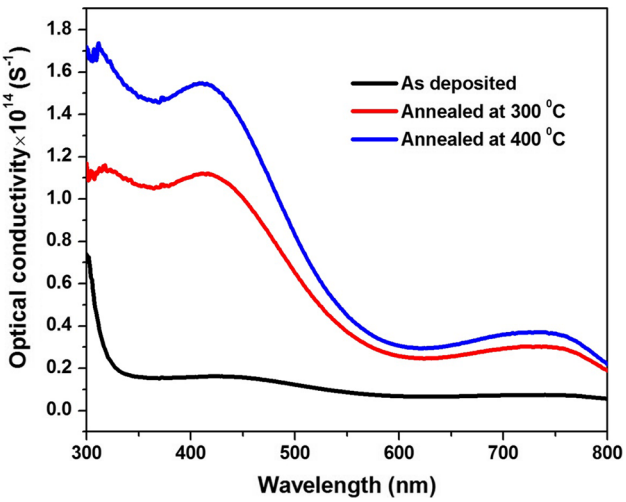

Fig. 12 Optical conductivity of Co_3O_4 thin films annealed at different temperatures

It is observed that the optical conductivity escalate with annealing temperatures. It is also to be pay attention, that the optical conductivity for all films are observed to show expansion in the high photon energies region and reduction in the low photon energy region, this reduction is because of the low absorbance of the films in that region.

3.4 I–V Characteristics of Co_3O_4 thin films

Exemplary room temperature current–voltage (I–V) characteristics of all the three films in the bias range of −3 to +3 V are shown in Fig. 13. A common factor observed in oxide materials is, exhibiting hysteretic nature due to the presence of large numbers of vacancies and defect sites

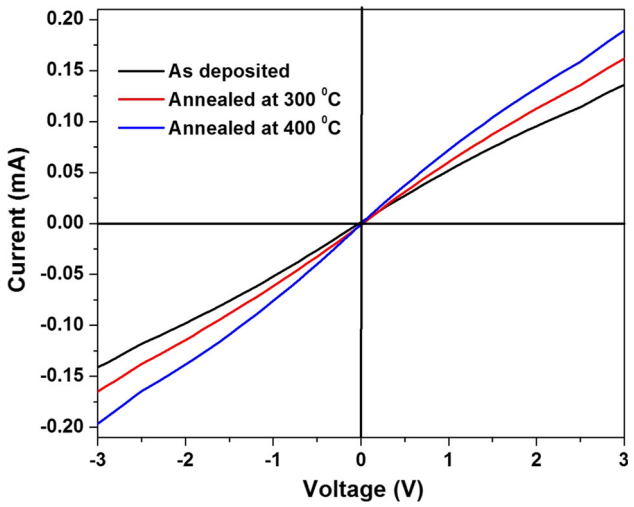

Fig. 13 Room temperature current–voltage characteristics of Co_3O_4 thin films annealed at different temperatures

cause trapping of charge carriers. The linear I–V characteristics passing through the origin, in the present case signifies the ohmic contact between the silver paste and the Co_3O_4 thin films. A bias is swept across the electrodes and the current passing through the samples is recorded. Exotically, I–V curves for all the three samples are straight and non-hysteretic. Linear I–V uniqueness is observed, which may be due to good grain to grain connectivity. The outcome of I–V characteristics revealed that there is decrement in resistance when there is increment in annealing temperature and is obtained for the sake of the grain size. When grain size grows into larger, it leads to enhanced movement of electron.

4 Conclusion

Co_3O_4 thin film was prepared onto glass substrate by spray pyrolysis using nebulizer technique. XRD patterns revealed the formation of cubic phase with (1 1 1) and (2 2 2) planes in all samples. Morphological studies exposed that the uniform morphology with spherical grains were covered with entire surface of the film. Optical characterization shows that the direct band gap energy was lying between 2.26 and 1.77 eV. The optical properties namely absorption coefficient, extinction coefficient and refractive index were found to increase with annealing temperature. The electrical studies show the increase in current with the increase of annealing temperature.

References

1. S. Elhag, Z.H. Ibupoto, O. Nour, M. Willander, Materials. **8**, 149–161 (2015)
2. X.H. Xia, J.P. Tu, J. Zhang, J.Y. Xiang, X.L. Wang, X.B. Zhao, Sol. Energy Mater. Sol. Cells. **94**, 386–389 (2010)
3. V. Patil, S. Pawar, M. Chougule, B. Raut, R. Mulik, S. Sen, Sens. Transducer. J. **128**(5), 100–114 (2011)
4. G. Wang, X. Shen, J. Horvat, B. Wang, H. Lui, D. Wexler, J. Yao, J. Phys. Chem. Part C Nanomater. Interface. **113**(11), 4357–4361 (2009)
5. L. Xue, C. Zhang, H. He, Y. Teraoka, Appl. Catal. B. Environ. **75**, 167–174 (2007)
6. T.T. Baby, R. Sundara, Mater. Chem. Phys. **135**(2–3), 623–627 (2012)
7. B.K.H. Maiyaly, I. A-Haitham, J. Pure Appl. Sci. **26**(1), 159–166 (2013)
8. C.U. Mordi, M.A. Eleruja, B.A. Taleatu, G.O. Egharevba, A.V. Adedeji, O.O. Akinwunmi, B. Olofinjana, C. Jeynes, E.O.B. Ajayi, J. Mater. Sci. Tech. **25**(1), 85–89 (2009)
9. V. Vannier, M. Schenk, K. Kohse-Hoinghaus, N. Bahlawane, J. Mater. Sci. **47**, 1348–1353 (2012)
10. D.U. Onah, C.E. Okeke, R.U. Osuji, B.A. Ezekoye, J.E. Ekpe, G.F. Ibeh, A.B.C. Ekwealor, F.I. Ezema, Chem. Mater. Sci. **3**(1), 43–51 (2013)
11. H. Tototzintle-Huitle, E. Prokhorov, A. Mendoza-Galvan, J.E. Urbina, J. Gonzalez-Hernandez, J. Phys. Chem. Solids. **64**, 975–980 (2003)
12. S. Oboudi, I.J. Inn, Res. Sci. Eng. Tech. **3**(1), 8573–8581 (2014)
13. V. Gowthami, M. Meenakshi, P. Perumal, R. Sivakumar, C. Sanjeeviraja, Int. J. Chem. Tech. Res. **6**(13), 5196–5202 (2014)
14. A.M.E. Raj, K.C. Lalithambika, V.S. Vidhya, G. Rajagopal, A. Thayumanavan, M. Jayachandran, C. Sanjeeviraja, Phys. B Condens. Matter **B403**, 544–554 (2008)
15. N. Sethupathi, P. Thirunavukkarasu, V.S. Vidhya, R. Thangamuthu, G.V.M. Kiruthika, K. Perumal, H.C. Bajaj, M. Jayachandran, J. Mater. Sci. Mater. Electron. **23**, 1087–1093 (2012)
16. S. Marikkannu, C. Sanjeeviraja, S. Piraman, A. Ayeshamariam, J Mater. Sci Mater. Electron. **26**, 2531–2537 (2015)
17. V.R. Shinde, S.B. Mahadik, T.P. Gujar, C.D. Lokhande, Appl. Surf. Sci. **252**, 7487–7492 (2006)
18. S. Parthiban, E. Elangovan, K. Ramamurthi, R. Martins, E. Fortunato, Sol. Energy Mater. Sol. Cells. **94**, 406–412 (2010)
19. R. Drasovean, S. Condurache-Bota, J. Optoelectron. Adv. Mater. **11**(12), 2141–2144 (2009)
20. V. Balouria, S. Samanta, A. Singh, A.K. Debnath, A. Mahajan, R.K. Bedi, D.K. Aswal, S.K. Gupta, Sens. Actuators B Chem. **176**, 38–45 (2013)
21. R.A. Chikwenze, M.N. Nnabuchi, J. Optoelectron. Adv. Mater. **12**, 2363–2368 (2010)